



# Effect of Tungsten Carbide Addition on the Wear Resistance of Flame-Sprayed Self-Lubricating Ni-Graphite Coatings

Zhaoxiang Chen, Hao Li, Limei Ren, Yunyu Li, and Changxin Liu

(Submitted July 24, 2019; in revised form December 22, 2019; published online February 6, 2020)

Ni-graphite coatings are widely used in industrial fields to improve the self-lubrication property of metallic surfaces. In this study, the effect of tungsten carbide (WC) addition on the microstructure, hardness and wear resistance of flame-sprayed Ni-graphite coatings was investigated. Microstructure examination of coatings shows that WC particles adhered well to Ni matrix but tended to come into contact with each other or graphite particles with the increasing addition amount. The hardness of the Ni-based graphite/WC composite coating depended on the WC content and reached its maximum at the WC addition amount of 30 wt.%. Tribological tests reveal that when the WC content was increased from 0 to 30 wt.%, the wear rate decreased about 42% (from about  $5.0 \times 10^{-5}$  to  $2.9 \times 10^{-5} \text{ mm}^3 \text{ N}^{-1} \text{ m}^{-1}$ ), while the maximum friction coefficient increased only about 19% (from about 0.16 to 0.19). The graphite in the coatings contributed to low friction coefficient with the formation of self-lubricating tribofilm. The wear mechanism of the coatings was mainly delamination, and well-embedded WC particles inhibited the propagation of delamination cracks. Results show that the Ni-based graphite/WC composite coating with 30 wt.% WC achieved a good balance between the wear resistance and the self-lubrication property.

**Keywords** flame spray, graphite, Ni-based coating, WC, wear resistance

## 1. Introduction

With the rapid development of mechanical industry, low friction and anti-wear have become important goals for designing and manufacturing machine parts (Ref 1, 2). Therefore, self-lubricating coatings or materials are increasingly used in the mechanical components to decrease the friction and wear (Ref 3-6). As a self-lubricating coating, the Ni-graphite coating has obtained successful application in aerospace. For example, Ni-graphite coatings used in the aircraft turbine compressors can maintain a small clearance between the rotating blades and shell to minimize the escape of compressed air and thus improve the engine efficiency (Ref 7-9). The nickel matrix in the Ni-graphite coating provides the necessary cohesion and adhesion strength, while the self-lubricating graphite phase can decrease the friction coefficient.

Although the self-lubrication effect of the Ni-graphite coating is good, its wear resistance needs to be improved

under the service condition of heavy load, such as in the mining or metallurgical machinery (Ref 10). In general, the wear resistance of Ni-based coatings can be improved by introducing reinforcing ceramic materials (Ref 11-13). But special attention should be paid to the compatibility between the reinforcing phase and the coating matrix. The reinforcing phase may be pulled out from the coating matrix during the friction process when the compatibility between them is poor, thereby causing severe third-body abrasion to friction pairs (Ref 14). Studies have proved that the WC particle has good compatibility or wettability with the Ni-based or Co-based coating matrix, and its high hardness, toughness and strong wear resistance are beneficial to the coatings (Ref 15).

The WC particles can be incorporated into the Ni-based coatings with many surface modification techniques such as the laser cladding and the thermal spray. The laser-cladded Ni-WC composite coatings usually have low porosity and strong adhesion to the substrate. However, the laser processing parameters must be precisely controlled to avoid the non-homogenous WC distribution as well as the dissolution of WC by melted Ni phase (Ref 16-18). In contrast, the operation of thermal spray is relatively simple. The commonly used thermal spray technologies for the deposition of Ni-based composite coatings include flame spray, atmospheric plasma spray, high-speed oxygen fuel spray, etc. (Ref 19-22). Among them, flame spray technology is popular due to its convenience, high output and low cost (Ref 21, 22). Usana-ampaipong et al. incorporated WC particles into the NiCrBSi coating using the flame spray technology. Microstructure observation showed that WC particles exhibited homogenous distribution in the deposited coating (Ref 21). Harsha et al. investigated the abrasive wear resistance of flame-sprayed Co-Cr-W-Ni-C coating with the WC addition. Results revealed that the addition of WC in a commercial powder coating could increase the wear resistance about 4-9 folds (Ref 22). At present, there are limited studies on

Zhaoxiang Chen, Hao Li, Yunyu Li, and Changxin Liu, School of Mechanical Engineering, Yanshan University, Qinhuangdao 066004, China; and Aviation Key Laboratory of Science and Technology on Generic Technology of Self-lubricating Spherical Plain Bearing, Yanshan University, Qinhuangdao 066004, China; Limei Ren, School of Mechanical Engineering, Yanshan University, Qinhuangdao 066004, China; and Key Laboratory of Advanced Forging and Stamping Technology and Science (Yanshan University), Ministry of Education of China, Qinhuangdao 066004, China. Contact e-mail: lmren@ysu.edu.cn.

the introduction of WC particles into the flame-sprayed Ni-graphite coating as well as the corresponding tribological performance characterization.

In this study, the Ni-based graphite/WC composite coatings were prepared on the stainless steel substrate by the flame spray technology. The proportion of spraying powders, including the Ni-coated graphite powders and the WC powders, was tuned to achieve improved wear resistance of the composite coating on the basis of preserving its self-lubrication property. The microstructure, hardness, bonding strength and tribological properties of the fabricated coatings were characterized and evaluated using scanning electron microscopy (SEM), x-ray diffraction (XRD), optical microscope, Vickers hardness tester, surface profiler, lap-shear test and reciprocating ball-on-plate friction and wear tester.

## 2. Materials and Methods

### 2.1 Specimen Preparation

A number of 304 stainless steel plates were used as the substrates. Prior to the spray process, all the substrate samples were treated by a grinding machine to increase their surface roughness, which can enhance the bonding strength between the coating and the substrate. The final roughness of the substrate sample was measured using a confocal optical profilometer (Conscan Profilometer, Anton-Paar Tritec SA, Peseux, Switzerland), and the measured average value was  $4.9 \pm 0.28 \mu\text{m}$ . After that, the substrate samples were cleaned in 95 wt.% alcohol ultrasonically for 30 min and dried at ambient temperature.

Ni-coated graphite powders (25 wt.% graphite coated by 75 wt.% Ni, Beijing Research Institute of Mining & Metallurgy, Beijing, China) were used for the spray deposition of Ni-graphite coatings. WC powders (Xin Dun Alloy Welding Material Spraying Corporation, Nangong, China) were added into the Ni-coated graphite powders for the spray deposition of Ni-based graphite/WC composite coatings. The addition amount of WC powders was set as 20, 30, 40 and 50 wt.%, respectively. All powders were screened by 150 mesh stainless steel screen. Then, they were mixed up in 95 wt.% alcohol, well stirred for 30 min and fully dried before the spray deposition. The coatings were fabricated using an oxyacetylene flame spray gun (Castodyn DS 8000, Poland). The parameters used for the coating deposition were set as follows: neutral flame (oxygen pressure of 0.4 MPa and acetylene pressure of 0.07 MPa) and air pressure of 0.2 MPa. The distance from the nozzle outlet to the substrate surface was 100 mm.

### 2.2 Characterization of Powders and Coatings

The microstructure of powders and coatings was characterized by scanning electron microscopy (SEM, SIGMA-500, ZEISS, Jena, Germany) equipped with energy-dispersive spectroscopy (EDS). For the cross-sectional observation, the powders and coatings were embedded in epoxy resin and polished with sandpapers. The EDS was used to analyze the elemental composition of powders and coatings. The phase structure of the coatings was determined by x-ray diffraction (XRD, D/MAX-2500/PC, RIGAKU, Tokyo, Japan). The XRD measurement was taken in the  $2\theta$  range of  $20^\circ$ – $80^\circ$  at a

scanning speed of  $2^\circ/\text{min}$ . The Vickers micro-hardness measurement was taken on the polished surface of the coatings using a Vickers hardness tester (FM-ARS 9000, FUTURE-TECH, Japan) under a load of 200 g.

### 2.3 Tribological Tests

The friction coefficient and wear behavior of the coatings were tested at ambient temperature under dry sliding condition by using a reciprocating ball-on-plate friction and wear tester (Tribometer, Anton-Paar Tritec SA, Peseux, Switzerland). The  $\text{Al}_2\text{O}_3$  ball of 6 mm in diameter was used as the counterpart material. The tribo-test was carried out under a normal load of 10 N with a sliding distance of 700 m and maximum speed of 0.1 m/s. Triplicate tribological tests were conducted for each sample to ensure repeatability. After the friction and wear test, the wear track was measured using the confocal optical profilometer mentioned above and a surface profiler (MarSurf, Mahr, Germany). The morphology and elemental composition of wear tracks were characterized using SEM/EDS. The wear rate  $K$  was determined by the following equation:  $K = (S \cdot l) / (F \cdot L)$ , where  $S$  is the cross-sectional area of wear track ( $\text{mm}^2$ ),  $l$  is the length of wear track (mm),  $F$  is the applied load (N), and  $L$  is the sliding distance (m).

### 2.4 Bonding Strength Test

The bonding strength of the coatings was measured via a lap-shear test (ASTM D1002). Each lap-shear specimen consisted of two same coating samples which were bonded together using a strong epoxy glue (Araldite<sup>®</sup> 2000 + Adhesives, Huntsman, USA). The overlapped area of two samples was  $25.4 \times 25.4 \text{ mm}^2$ . Coatings used for this test were thick (about  $380 \mu\text{m}$ ) enough to prevent penetration of liquid glue through the coating. The tensile test was performed using a universal material testing machine (WDW-100E, Koohei, Jinan, China) at a constant crosshead speed of 1.3 mm/min. The tensile load was applied parallel to the coating/substrate interface to induce the detachment of the coatings. The maximum tensile load divided by the overlapped area was herein denoted as the shear bonding strength of the coatings, and five lap-shear specimens were measured for each condition.

## 3. Results and Discussion

### 3.1 Characterization of Powders

Figure 1 presents the cross-sectional morphologies of Ni-coated graphite powders and WC powders. It can be seen that two kinds of powders both exhibited irregular shape, which can promote the mechanical interlocking between them. The elemental composition of two kinds of powders is shown in Table 1. From Fig. 1(a) and Table 1, it can be seen that the Ni-coated graphite powder consisted of inner graphite particle (point P1) and outer Ni material (point P2). The outer Ni material can protect the inner graphite particle from being oxidized during the spray process. From Fig. 1(b), it can be seen that some WC particles were partly broken due to the grinding and polishing process of the SEM sample. And the elemental composition analysis of point P3 (see Fig. 1b and Table 1) verified the purity of WC powders used in this study.

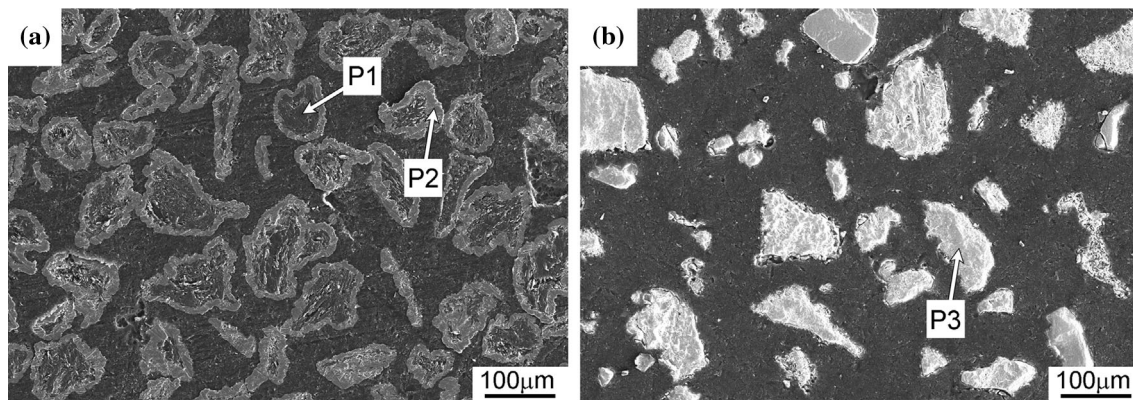


**Fig. 1** Cross-sectional morphologies of spraying powders: (a) Ni-coated graphite powders; (b) WC powders

**Table 1** The elemental composition of the Ni-coated graphite powder and the WC powder

Point	Element, wt.%		
	Ni	C	W
P1	3.79	96.21	...
P2	96.68	3.32	...
P3	...	8.37	91.63

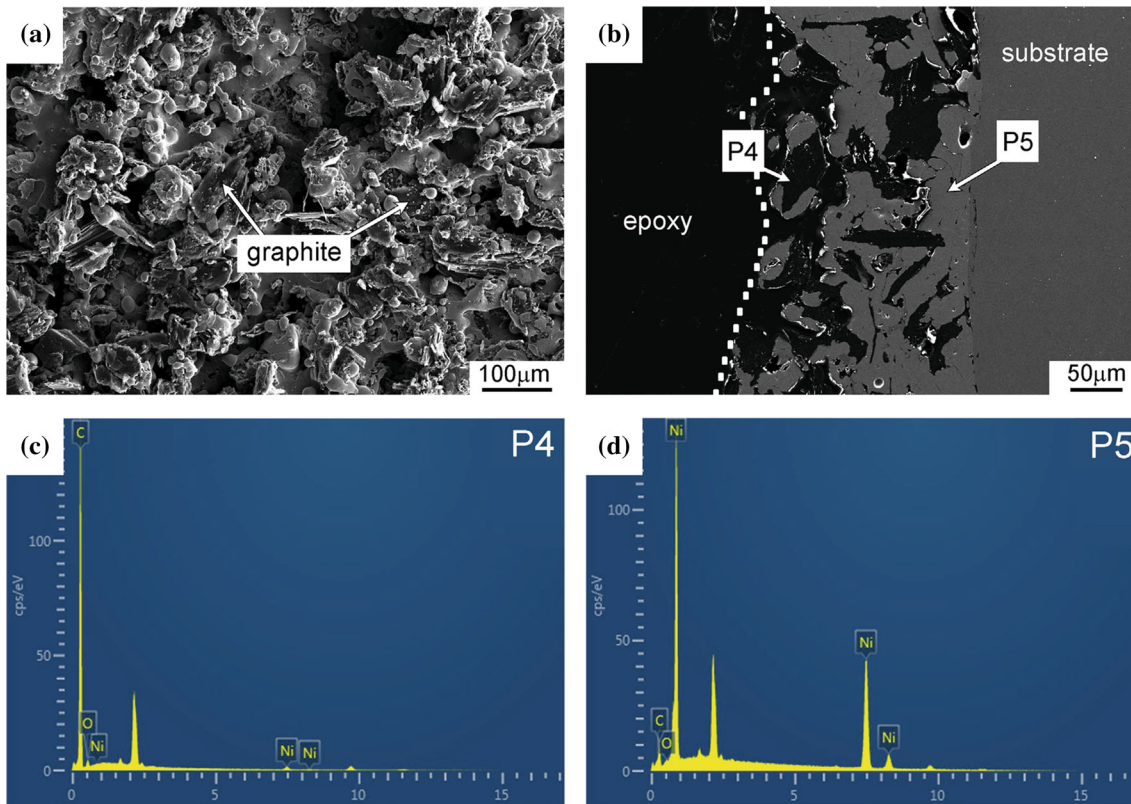
### 3.2 Microstructure, Composition and Hardness of Coatings

Figure 2 shows the surface and cross-sectional morphologies of the Ni-graphite coating and EDS analysis results. It can be observed from Fig. 2a that the Ni-graphite coating exhibited typical rough surface of flame-sprayed coatings. During the spray process, the inner layer of the coating was deposited on the sample first, and then, it was impacted continuously by the subsequent particles, while the surface layer was not subjected to such repeating particle impingement. Therefore, the surface layer of the coating possessed a relatively loose structure. In addition, there was graphite being exposed on the coating surface, as indicated by arrows in Fig. 2a. This was caused by the flame-heating effect. The Ni-coated graphite powders were heated by the flame so that the outer Ni material became semi-molten or molten, while the inner graphite particle remained solid due to its higher melting point (Ref 23). When these heated powders impacted on the sample surface, the outer molten Ni material and the inner solid graphite were easy to depart from each other, leading to the exposure of interior graphite particle. Similar phenomenon was also observed on the surface of plasma sprayed Ni-graphite coatings (Ref 9). In contrast, most graphite particles were well wrapped by continuous outer Ni films in the cold sprayed Ni-Al-graphite coatings (Ref 24).

The cross-sectional morphology of the Ni-graphite coating and EDS analysis results of selected phases (see point P4 and P5) are shown in Fig. 2(b), (c) and (d), respectively. It can be seen that the dark area in the coating was mainly composed of graphite particles (Fig. 2b and c), while the gray area corresponded to Ni matrix (Fig. 2b and d). The unmarked peaks in Fig. 2(c) and (d) were assigned to gold element, which was from the gold layer on the SEM sample surface for better

electrical conductivity. It can be seen that graphite particles exhibited relatively uniform distribution in the coating and adhered well to Ni matrix. This benefited from the adoption of Ni-coated graphite powders. First, the outer Ni material promoted graphite particles to be isolated from each other. Secondly, the outer Ni material can effectively protect most graphite particles from being oxidized during the spray process. However, there were still some graphite particles coming into direct contact with each other in the deposited coating, as shown in Fig. 2(b). On the one hand, the closer the graphite particles are to each other, the easier to form a lubricating graphite film during the friction and wear process, which will function a better lubricating effect (Ref 9). On the other hand, the interconnected graphite particles decreased the continuity of the Ni matrix and promoted the formation of voids or cracks in the coating, which had a negative impact on the wear resistance and bonding strength of the Ni-graphite coating.

The WC particles were incorporated into the Ni-graphite coating to improve the wear resistance. The addition amount of WC in the feed powders was set as 20, 30, 40 and 50 wt.%, respectively. As mentioned above, WC particle has good compatibility with the nickel, but its addition amount must be moderate in order to guarantee the cohesion and adhesion strength of the Ni-based coating. The surface and cross-sectional morphologies of Ni-based graphite/WC composite coatings and EDS analysis results of the selected phase are shown in Fig. 3. From Fig. 3(a), it can be seen that the Ni-based graphite/WC coating with 30 wt.% WC had similar surface morphology to the Ni-graphite coating. The difference between them is that there existed WC particles on the surface of the Ni-based graphite/WC coating. From Fig. 3(b), it can be seen that the Ni-based graphite/WC coating also contained gray Ni matrix phase and dark graphite phase. Besides, a new phase in white contrast is observed in Fig. 3(b) and the EDS analysis result of point P6 verified that the white phase was WC particle (see Fig. 3c). The WC particle was embedded in the composite coating and adhered well to the surrounding Ni matrix, without sign of melting or dissolution. The good compatibility and adhesion between the WC and Ni matrix are beneficial to wear resistance of the coating (Ref 19). In contrast, considerable WC dissolution into the metal matrix tended to occur in the laser-cladded composite coatings, which could impair the coating's wear resistance (Ref 16). When the addition amount of WC in the feed powder was further increased up to 50 wt.%, more WC



**Fig. 2** Surface (a) and cross-sectional (b) morphologies of the Ni-graphite coating and (c, d) EDS analysis results of selected phases

particles could be observed in the coating, as shown in Fig. 3(d). The increased WC content was accompanied with the decreased content of Ni matrix so that WC particles in the coating began to come into contact with each other or graphite particles.

In addition, it can be noted from Fig. 2 and 3 that the thickness of coating decreased after the addition of WC particle. Specifically, the average thickness of coatings with 0, 30 and 50 wt.% WC was  $186.5 \pm 21.7$ ,  $162.6 \pm 21.0$  and  $154.0 \pm 11.2$   $\mu\text{m}$ , respectively. This is partly because that the WC particle has higher density than the Ni-coated graphite particle. During the spraying operation, high-density WC particles provided more forceful impingement on the deposited coating and thus resulted in denser coating structure and decreased coating thickness. For the industrial application, the coating thickness can be optimized by adjusting the spray parameters to achieve longest service life.

Figure 4 shows the XRD patterns of sprayed coatings. The detected phases in the Ni-graphite coating mainly consisted of graphite,  $\gamma$ -Ni and NiO (curve a in Fig. 4). The formation of NiO phase in the coating was attributed to the fact that the Ni material was partially oxidized during the flame spray process. After WC particles were incorporated into the Ni-graphite coating, the formed composite coating exhibited different phase constitution. Take the composite coating with 50 wt.% WC for example, the new phase of WC could be detected in the coating (curve b in Fig. 4). This result is consistent with the

microstructure observation and composition analysis shown in Fig. 3(c).

Figure 5 shows the average hardness of Ni-based graphite/WC composite coatings with different WC contents. It can be seen that with the increase in WC content, the hardness of the composite coating rose at first and went down later. Before the WC addition, the coating hardness was about  $195 \pm 10$   $\text{HV}_{200\text{g}}$ . When the WC content was increased up to 30 wt.%, the hardness of the composite coating reached a peak value of  $318 \pm 16$   $\text{HV}_{200\text{g}}$ . The increased hardness had to do with the improved phase constitution and microstructure of the composite coating. As mentioned above, the Ni-based graphite/WC coating mainly consisted of the hard phase of WC, soft phase of graphite and matrix phase of Ni. When the WC content was moderate, hard WC particles could form good adhesion to the Ni matrix (see Fig. 3b), which inhibited crack propagation during the indentation test because cracks were difficult to propagate into the WC/Ni interface or penetrate into the hard WC particle. On the contrary, cracks were easier to initiate and propagate in the soft graphite phase due to its typical lamellar structure. Therefore, with the initial increase in WC content and the corresponding decrease in graphite content, the composite coating exhibited improved fracture toughness and hardness. However, when the WC content was further increased beyond 30 wt.%, the reinforcing effect of hard WC phase became weakened. It can be seen that the hardness of the composite coating with 50 wt.% WC decreased to  $196 \pm 44$   $\text{HV}_{200\text{g}}$ , close to the composite coating without WC addition. This is

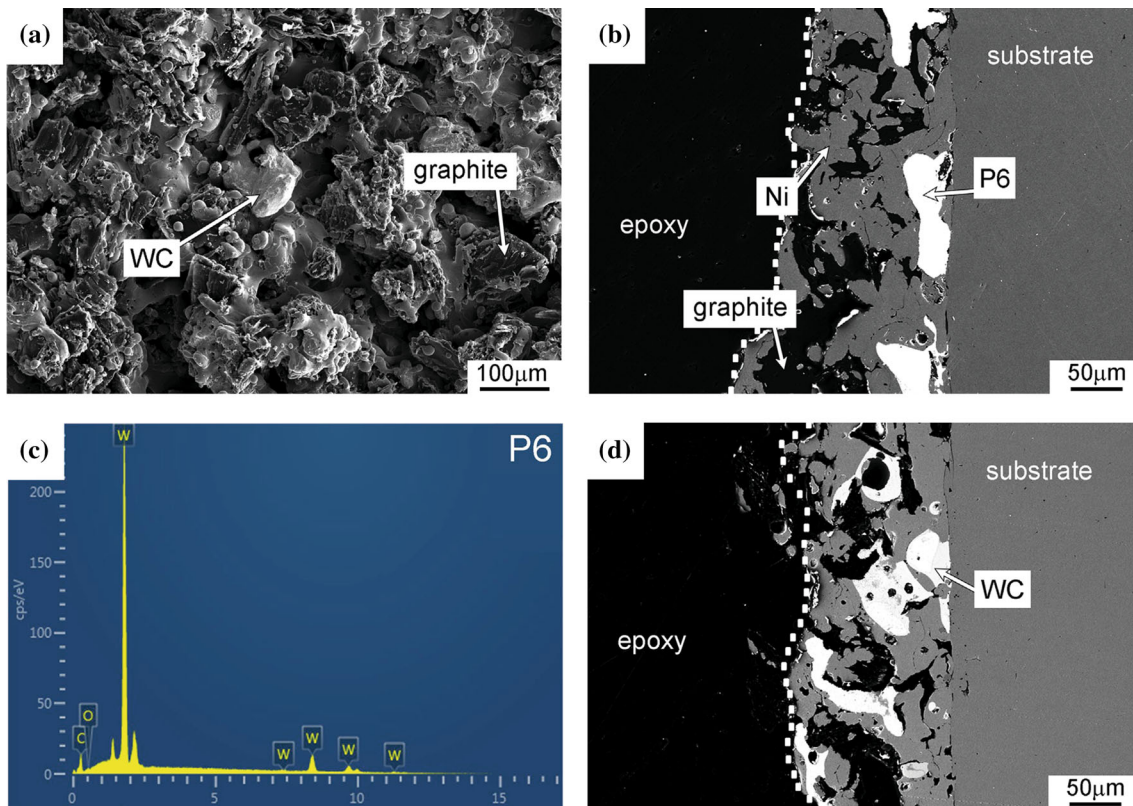


**Fig. 3** Surface and cross-sectional morphologies of Ni-based graphite/WC composite coatings and EDS analysis result of the selected phase: (a–c) the composite coating with 30 wt.% WC; (d) the composite coating with 50 wt.% WC

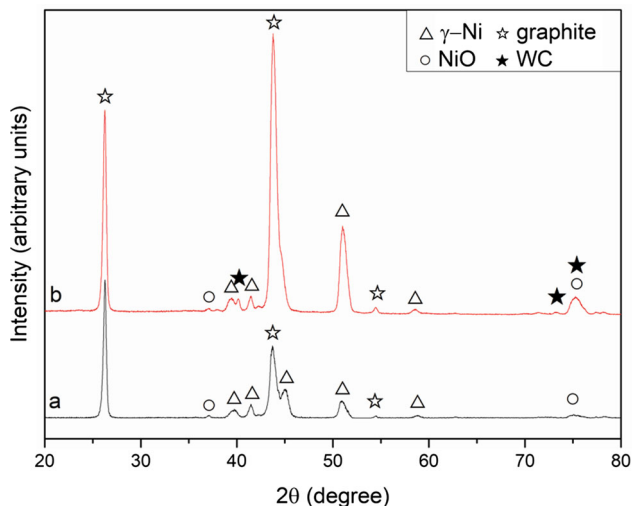


**Fig. 4** XRD patterns of sprayed coatings: (a) Ni-graphite coating; (b) Ni-based graphite/WC composite coating with 50 wt.% WC

related to the decreased content of bonding Ni matrix phase. Comparing Fig. 3(b) with (d), it can be seen that when the WC content was increased up to 50 wt.%, more WC particles began to come into direct contact with each other or graphite particles due to less Ni material in the coating. The adhesion between WC and graphite particles was weak without the sufficient bonding of Ni matrix so that the composite coating was easier to be crushed under the indentation load, resulting in decreased hardness.

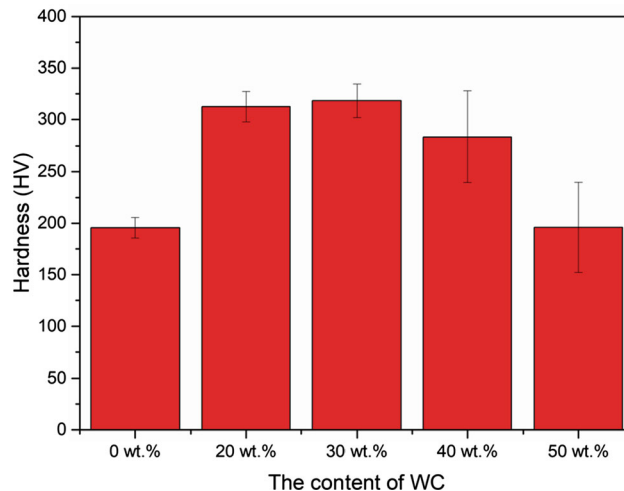


**Fig. 5** Hardness of Ni-based graphite/WC composite coatings with different WC contents

### 3.3 Tribological Properties and Bonding Strength of Coatings

Figure 6 shows the tribological test results of Ni-based graphite/WC composite coatings with different WC contents. The tribological properties were measured at ambient temperature under the dry sliding condition by using a ball-on-plate reciprocating tribometer. The tribo-tests were carried out at the normal load of 10 N with an  $Al_2O_3$  grinding ball as the counterpart.

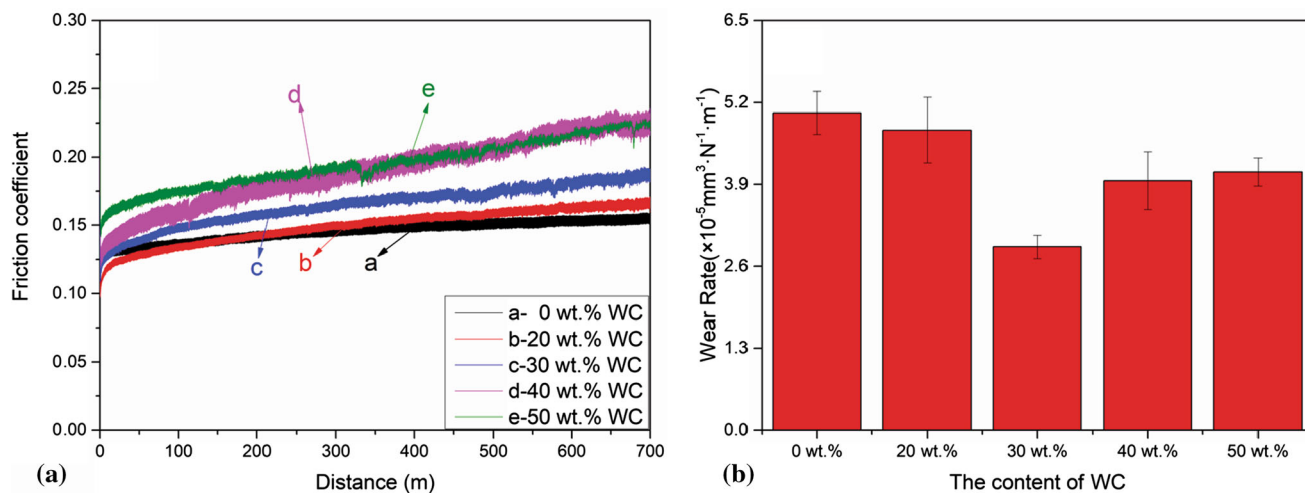


**Fig. 6** Friction coefficient (a) and wear rate (b) of Ni-based graphite/WC composite coatings with different WC contents

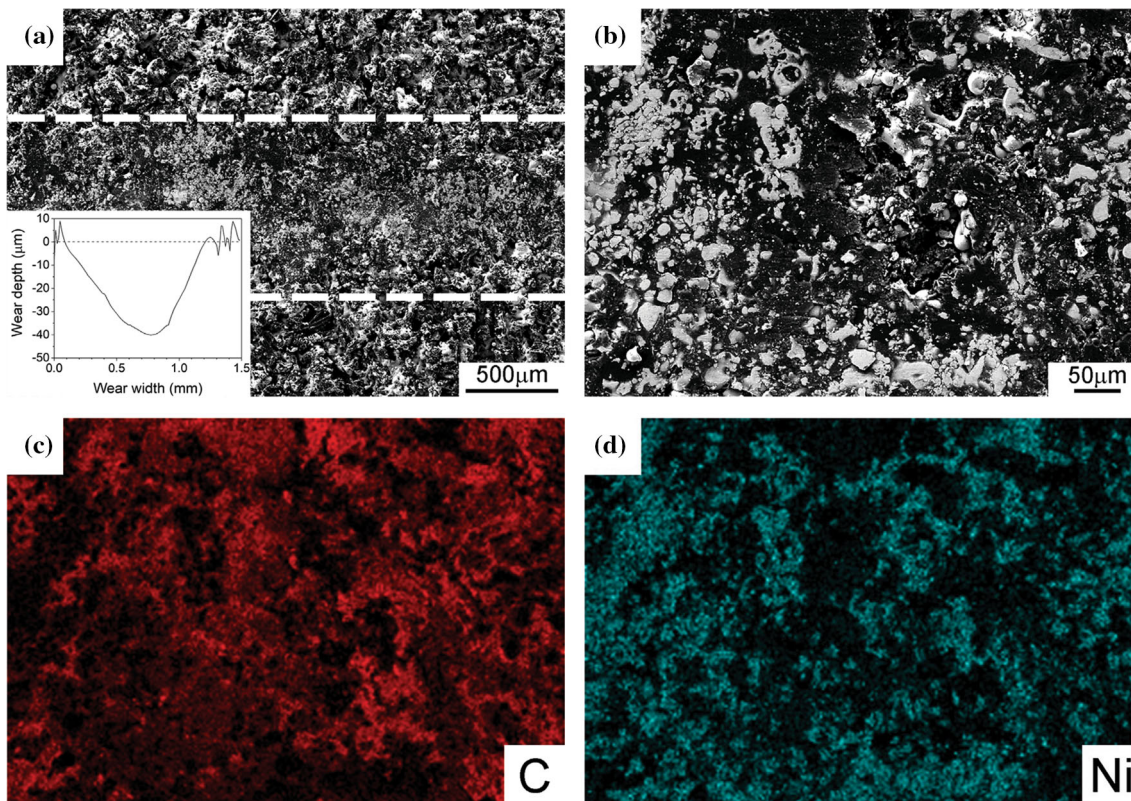
Figure 6a shows the friction coefficient of Ni-based graphite/WC composite coatings with different WC contents. As can be seen, when the WC content was less than or equal to 20 wt.%, the friction coefficient of coatings was close to each other, including their variation tendency and magnitude. Specifically, the friction coefficient of the coatings achieved relatively stable (in the range from about 0.14 to 0.16) within a short sliding distance of about 150 m. This suggests that there was enough graphite in these two kinds of coatings to quickly form a self-lubricating tribofilm between the friction pairs. Tang et al. (Ref 9) measured the average friction coefficient of atmospheric plasma-sprayed Ni-graphite coatings and obtained similar result (about 0.17). For the composite coating with 30 wt.% WC, although its friction coefficient exhibited a continuously rising trend with the sliding distance, the rising speed was very low and the maximum friction coefficient was about 0.19, only slightly larger than that of the composite coating without WC addition (with a maximum value of about 0.16). This means that despite the decreased graphite content in the composite coating with 30 wt.% WC, an effective self-lubricating tribofilm still could be formed during the friction process. However, when the WC content was increased up to 40 wt.% or more, the friction coefficient of the coating rose rapidly and reached a high value of about 0.23.

Figure 6(b) shows the wear rate of Ni-based graphite/WC composite coatings with different WC contents. It can be seen that the wear rate of the composite coating decreased significantly from  $5.03 \pm 0.34 \times 10^{-5}$  to  $2.90 \pm 0.18 \times 10^{-5} \text{ mm}^3 \text{ N}^{-1} \text{ m}^{-1}$  with the increased WC content from 0 to 30 wt.%. Significant improvement in wear resistance of the Ni-based coatings with the WC addition was also reported in previous studies (Ref 25, 26). For example, Alidokht et al. reported a decreased wear rate from about  $4.0 \times 10^{-5}$  to  $6 \times 10^{-6} \text{ mm}^3 \text{ N}^{-1} \text{ m}^{-1}$  after the 10.5 vol.% WC addition in the cold sprayed Ni coating (Ref 26). From Fig. 6(a) and (b), it can be seen that when the WC content was within the range from 0 to 30 wt.%, the wear rate of the composite coating was more sensitive to the change of WC content than the friction coefficient. The average wear rate decreased about 42%, while the maximum friction coefficient only increased about 19%. Beyond 30 wt.%, both the wear rate and the friction coefficient of the composite coating exhibited a

rising trend, indicating the decreased wear resistance and self-lubrication property. This result suggests that the Ni-based graphite/WC composite coating with 30 wt.% WC possessed the lowest wear rate and an acceptable friction coefficient, keeping a good balance between the wear resistance and the self-lubrication property.

The bonding strength of the coatings was measured via the lap-shear test. Results show that the coating with 30 wt.% WC had slightly higher bonding strength ( $10.31 \pm 1.53 \text{ MPa}$ ) than the coating without WC ( $8.14 \pm 1.33 \text{ MPa}$ ). The present measured values are comparable with reported data. Ziegelheim et al. reported varied adhesion strengths of Ni-graphite coatings from 6.7 to 15.7 MPa depending on the flame spraying parameters (Ref 27), and Xu et al. (Ref 28) reported lower adhesion strength of about 5.2 MPa for a thick Ni-graphite coating (about 2 mm in thickness).

To clearly characterize the wear behavior of Ni-based graphite/WC composite coatings with different WC contents, the worn surfaces were examined by SEM/EDS. Figure 7 exhibits the worn morphology and corresponding EDS elemental maps of the Ni-graphite coating. As shown in Fig. 7(a) and (b), the worn surface featured with flattened dark patches and detached gray debris. The EDS analysis results (Fig. 7c and d) suggest that the dark patches mainly corresponded to graphite and the gray debris was mainly composed of Ni. The graphite particles were easily deformed and delaminated under the tangential friction force due to its soft nature and hexagonal structure. Accordingly, flattened graphite patches and continuous self-lubricating graphite tribofilm were observed on the wear track (Fig. 7b and c). This explains why the Ni-graphite coating possessed the lowest friction coefficient. The formation of Ni wear debris on the wear track was caused by two reasons. First, the Ni material was easy to yield under the normal load and tangential friction force and then may be torn off from the coating surface. Besides, the interfacial bonding between the deposited Ni splats or between the Ni material and graphite particle was relatively weak, and the friction-induced delamination cracks tended to propagate along these weak interfaces, promoting the detachment of Ni material. Therefore, the wear mechanism of the coatings was mainly delamination of coating materials along weak interfaces. The cross-sectional profile of the wear track (see the inset in Fig. 7a) shows that the wear



**Fig. 7** Worn morphology and corresponding EDS elemental maps of the Ni-graphite coating: (a) morphology and cross-sectional profile of the wear track; (b) high-magnification view of (a); (c) C map and (d) Ni map corresponding to (b)

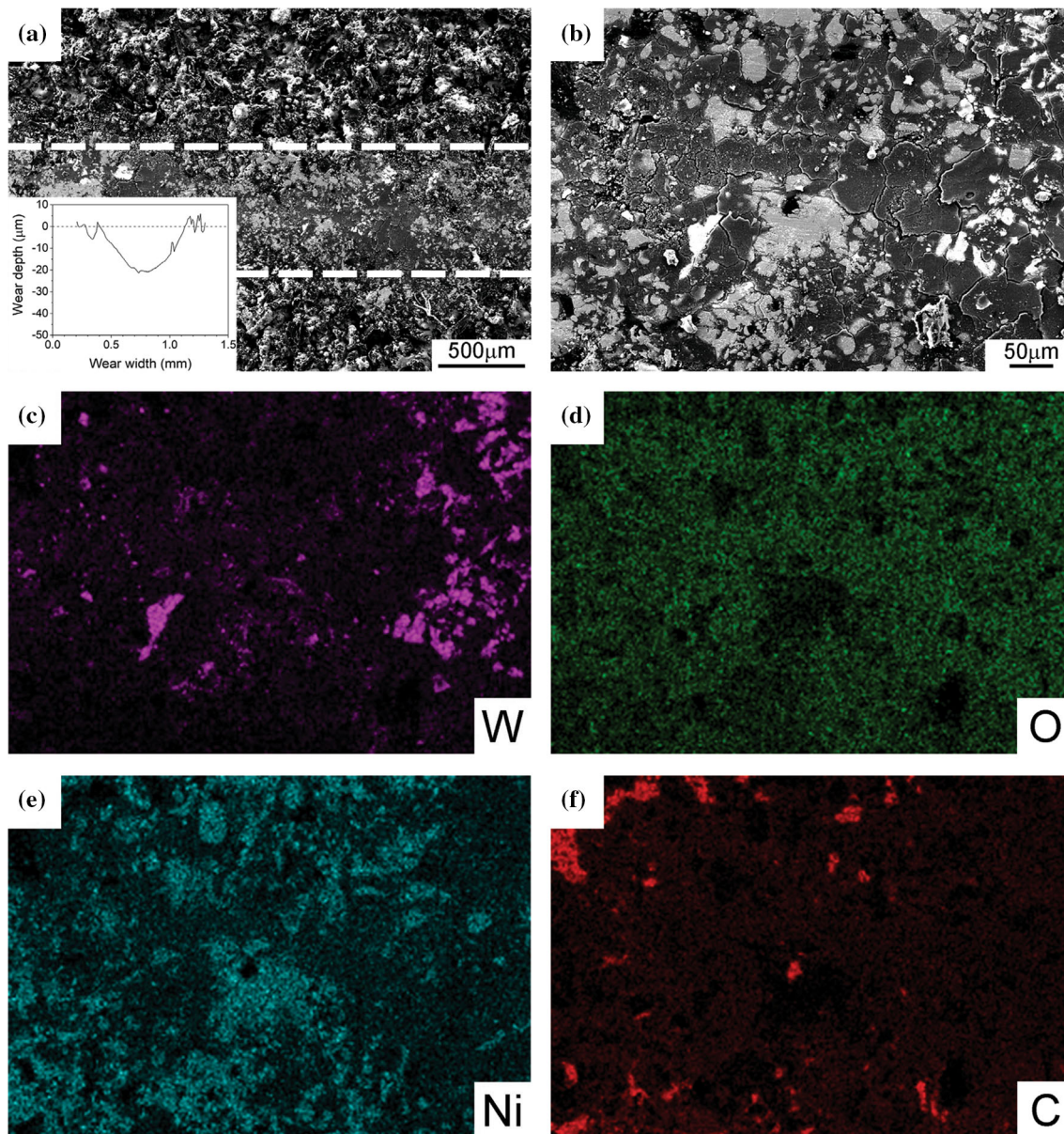
width was very wide (about 1.1 mm) and the maximum wear depth was near 40  $\mu\text{m}$ , indicating that the wear resistance of the Ni-graphite coating was poor, which is consistent with the high wear rate shown in Fig. 6b.

Figure 8 presents the worn morphology and corresponding EDS elemental maps of the Ni-based graphite/WC composite coating with 30 wt.% WC. For this coating, the worn surface exhibited different morphology from the Ni-graphite coating. As shown in Fig. 8, the worn surface was relatively smooth and featured with white WC particles, gray Ni matrix, dark gray lamellas and many micro-cracks. According to EDS elemental maps, the dark gray lamellas mainly consisted of O, Ni and C elements, resulting from the oxidized Ni debris and the graphite particles. During the wear test, the Ni and graphite materials on the coating surface were preferentially worn off, and thus, WC particles rose well above the surface gradually. The detached material debris first squeezed up against the embossed WC particles. Then, the debris became smooth and lamellar gradually under the repeated rolling of the alumina counterpart, as shown in Fig. 8(b). Similar wear phenomenon was also reported in previous studies (Ref 25, 26). In the meantime, the formed lamellas were partially oxidized due to the increased temperature at the friction surface. Such dark gray lamellas played a beneficial role in improving the coating wear resistance because they can prevent the alumina counterpart from further wearing the underlying coating matrix. There were little pulled-out WC particles detected on the wear track, indicating good adhesion between the WC particle and the Ni matrix. These well-embedded WC particles in the coating inhibited the propagation of delamination cracks and thus alleviated the detachment of coating materials.

From the C map shown in Fig. 8(f), it can be seen that the formed graphite self-lubricating tribofilm was less continuous and uniform due to the decreased graphite content in the composite coating. This explains why the Ni-based graphite/WC composite coating had higher friction coefficient than the Ni-graphite coating. But it is worth noting that the maximum friction coefficient was still relatively low (about 0.19) for the Ni-based graphite/WC composite coating with 30 wt.% WC. The cross-sectional profile of the wear track (see the inset in Fig. 8a) exhibited a much narrower and shallower wear track. The width of the wear track was about 0.7 mm, and the depth was about 21  $\mu\text{m}$ , suggesting the increased wear resistance compared with the Ni-graphite coating. Thereby, the Ni-based graphite/WC composite coating with 30 wt.% WC not only improved the hardness and wear resistance of the Ni-graphite coating, but also preserved its self-lubrication property. When the addition amount of WC exceeded 30 wt.%, too much WC particles would smash the continuity and uniformity of the Ni matrix and then led to weakness and fragility of the composite coating, resulting in increased wear rate. Thus, the best wear resistance of the Ni-based graphite/WC composite coating was obtained at an optimal WC addition amount of 30 wt.%.

## 4. Conclusions

In this study, the Ni-based graphite/WC composite coatings with different WC addition amounts were successfully prepared on the stainless steel substrate by the flame spray technology. The microstructure, hardness and tribological behavior of the



**Fig. 8** Worn morphology and corresponding EDS elemental maps of the Ni-based graphite/WC composite coating with 30 wt.% WC: (a) morphology and cross-sectional profile of the wear track; (b) high-magnification view of (a); (c) W map, (d) O map, (e) Ni map and (f) C map corresponding to (b)

coatings were investigated and compared to address the effect of WC content on the coating's wear resistance and self-lubrication property. The main conclusions are drawn as follows:

1. The flame-sprayed Ni-based graphite/WC composite coating mainly consisted of hard phase of WC, soft phase of graphite and matrix phase of Ni, as well as some NiO phase. The WC particles adhered well to Ni matrix without sign of melting or dissolution.
2. When the WC addition amount was in the range from 0 to 30 wt.%, the hardness and wear resistance of the Ni-based graphite/WC composite coating increased with the increasing WC content. Beyond that, both the hardness and the wear resistance of the composite coating decreased.

3. The Ni-based graphite/WC composite coating with 30 wt.% WC possessed highest wear resistance coupled with relatively low friction coefficient.

#### Acknowledgment

This research was supported by the Science and Technology Research Foundation in University (QN2019013), Returned Overseas Chinese Talents Foundation (CL201726) and Natural Science Foundation (E2016203270) of Hebei Province and the Fundamental Research Foundation (020000904) and Doctoral Foundation (B942) of Yanshan University.



## References

1. V.W. Wong and S.C. Tung, Overview of Automotive Engine Friction and Reduction Trends-Effects of Surface, *Material, and Lubricant-Additive Technologies*, *Friction*, 2016, **4**, p 1–28. <https://doi.org/10.1007/s40544-016-0107-9>
2. A. Tyagi, R.S. Walia, Q. Murtaza, S.M. Pandey, P.K. Tyagi, and B. Bajaj, A Critical Review of Diamond Like Carbon Coating for Wear Resistance Applications, *Int. J. Refract. Met. Hard Mater.*, 2019, **78**, p 107–122. <https://doi.org/10.1016/j.ijmhm.2018.09.006>
3. S. Zhu, J. Cheng, Z. Qiao, and J. Yang, High Temperature Solid-Lubricating Materials: a Review, *Tribol. Int.*, 2019, **133**, p 206–223. <https://doi.org/10.1016/j.triboint.2018.12.037>
4. M. Khadem, O.V. Penkov, H.K. Yang, and D.E. Kim, Tribology of Multilayer Coatings for Wear Reduction: A Review, *Friction*, 2017, **5**, p 248–262. <https://doi.org/10.1007/s40544-017-0181-7>
5. Z.X. Chen, X.P. Ren, L.M. Ren, T.C. Wang, and X.W. Qi, Improving the Tribological Properties of Spark-Anodized Titanium by Magnetron Sputtered Diamond-Like Carbon, *Coatings*, 2018, <https://doi.org/10.3390/coatings8020083>
6. L.M. Ren, T.C. Wang, Z.X. Chen, Y.Y. Li, and L.H. Qian, Self-Lubricating PEO-PTFE Composite Coating on Titanium, *Metals*, 2019, <https://doi.org/10.3390/met9020170>
7. R. Soltani, M. Heydarzadeh-Sohi, M. Ansari, F. Afsari, and Z. Valefi, Effect of APS Process Parameters on High-Temperature Wear Behavior of Nickel-Graphite Abradable Seal Coatings, *Surf. Coat. Technol.*, 2017, **321**, p 403–408. <https://doi.org/10.1016/j.surfcoat.2017.05.004>
8. W.H. Xue, S.Y. Gao, D.L. Duan, L. Wang, Y. Liu, and S. Li, Study on The High-Speed Rubbing Wear Behavior Between Ti6Al4V Blade and Nickel-Graphite Abradable Seal Coating, *J. Tribol. T. ASME*, 2017, <https://doi.org/10.1115/1.4033454>
9. J.J. Tang, K. Liu, Q.Z. Yang, Y.H. Wang, P. Zhang, Y. Wang, L. Zhao, Q.Q. Fu, Z.H. Han, and Y. Bai, The Influence of Size and Distribution of Graphite on the Friction and Wear Behavior of Ni-Graphite Coatings, *Surf. Coat. Technol.*, 2014, **252**, p 48–55. <https://doi.org/10.1016/j.surfcoat.2014.04.063>
10. B. Cai, Y.F. Tan, Y.Q. Tu, X.L. Wang, and H. Tan, Tribological Properties of Ni-Base Alloy Composite Coating Modified by Both Graphite and TiC Particles, *Trans. Nonferrous Met. Soc. China*, 2011, **21**, p 2426–2432. [https://doi.org/10.1016/s1003-6326\(11\)61031-5](https://doi.org/10.1016/s1003-6326(11)61031-5)
11. T. Chen, F. Wu, H.J. Wang, and D.F. Liu, Laser Cladding In-situ Ti(C, N) Particles Reinforced Ni-Based Composite Coatings Modified with CeO<sub>2</sub> Nanoparticles, *Metals*, 2018, **8**, p 4. <https://doi.org/10.3390/met8080601>
12. S.M. Huang, D.Q. Sun, W.Q. Wang, and H.Y. Xu, Microstructures and Properties of In-situ TiC Particles Reinforced Ni-Based Composite Coatings Prepared by Plasma Spray Welding, *Ceram. Int.*, 2015, **41**, p 12202–12210. <https://doi.org/10.1016/j.ceramint.2015.06.041>
13. M.A. Farrokhzad and T.I. Khan, Sliding Wear Performance of Nickel-Based Cermet Coatings Composed of WC and Al<sub>2</sub>O<sub>3</sub> Nanosized Particles, *Surf. Coat. Technol.*, 2016, **304**, p 401–412. <https://doi.org/10.1016/j.surfcoat.2016.07.014>
14. J. Yang, Y.J. Zhang, X.Q. Zhao, Y.L. An, H.D. Zhou, J.M. Chen, and G. Hou, Tribological Behaviors of Plasma Sprayed CuAl/Ni-Graphite Composite Coating, *Tribol. Int.*, 2015, **90**, p 96–103. <https://doi.org/10.1016/j.triboint.2015.04.022>
15. I. Konyashin, A.A. Zaitsev, D. Sidorenko, and E.A. Levashov, Wettability of Tungsten Carbide by Liquid Binders in WC-Co Cemented Carbides: Is It Complete for All Carbon Contents?, *Int. J. Refract. Met. Hard Mater.*, 2017, **62**, p 134–148. <https://doi.org/10.1016/j.ijmhm.2016.06.006>
16. P. Wu, H.M. Du, X.L. Chen, Z.Q. Li, H.L. Bai, and E.Y. Jiang, Influence of WC Particle Behavior on the Wear Resistance Properties of Ni-WC Composite Coatings, *Wear*, 2004, **257**, p 142–147. <https://doi.org/10.1016/j.wear.2003.10.019>
17. M.R. Fernández, A. García, J.M. Cuetos, R. González, A. Noriega, and M. Cadenas, Effect of Actual WC Content on the Reciprocating Wear of a Laser Cladding NiCrBSi Alloy Reinforced with WC, *Wear*, 2015, **324-325**, p 80–89. <https://doi.org/10.1016/j.wear.2014.12.021>
18. J.S. Xu, X.C. Zhang, F.Z. Xuan, Z.D. Wang, and S.T. Tu, Microstructure and Sliding Wear Resistance of Laser Cladded WC/Ni Composite Coatings with Different Contents of WC Particle, *J. Mater. Eng. Perform.*, 2012, **21**, p 1904–1911. <https://doi.org/10.1007/s11665-011-0109-8>
19. X. Wang, L.F. Zhu, Z.M. Zhou, G. Liu, E.Y. Liu, and Z.X. Zeng, Tribological Properties of WC-Reinforced Ni-Based Coatings under Different Lubricating Conditions, *J. Therm. Spray Technol.*, 2015, **24**, p 1323–1332. <https://doi.org/10.1007/s11666-015-0290-7>
20. T.A. Ben Mahmud, A.M. Atieh, and T.I. Khan, The Wear Behavior of HVOF Sprayed Near-Nanostructured WC-17%Ni(80/20)Cr Coatings in Dry and Slurry Wear Conditions, *J. Mater. Eng. Perform.*, 2017, **26**, p 3507–3515. <https://doi.org/10.1007/s11665-017-2739-y>
21. T. Usana-ampaipong, C. Dumkum, K. Tuchinda, V. Tangwarodomnukun, B. Teeraprawatekul, and H. Qi, Surface and Subsurface Characteristics of NiCrBSi Coating with Different WC Amount Prepared by Flame Spray Method, *J. Therm. Spray Technol.*, 2019, **28**, p 580–590. <https://doi.org/10.1007/s11666-019-00839-3>
22. S. Harsha, D.K. Dwivedi, and L. Geng, Research of Laser Addition in Co-Cr-W-Ni-C Flame Sprayed Coatings on Microstructure, Microhardness and Wear Behaviour, *Surf. Coat. Technol.*, 2006, **201**, p 5766–5775. <https://doi.org/10.1016/j.surfcoat.2006.10.026>
23. S.Q. Yang, Q.W. Meng, and L. Geng, Research of Laser Remelting Nickel-Coated Graphite Layer on Titanium Alloy Substrate, *Appl. Laser*, 2006, **26**, p 227–229. <https://doi.org/10.3969/j.issn.1000-372x.2006.04.004> (in Chinese)
24. C.J. Huang, W.Y. Li, M.P. Planche, H.L. Liao, and G. Montavon, In-situ Formation of Ni-Al Intermetallics-Coated Graphite/Al Composite in a Cold-Sprayed Coating and Its High Temperature Tribological Behaviors, *J. Mater. Sci. Technol.*, 2017, **33**, p 507–515. <https://doi.org/10.1016/j.jmst.2017.01.026>
25. K. Van Acker, D. Vanhoyweghen, R. Persoons, and J. Vangrunderbeek, Influence of Tungsten Carbide Particle Size and Distribution on the Wear Resistance of Laser Clad WC/Ni Coatings, *Wear*, 2005, **258**, p 194–202. <https://doi.org/10.1016/j.wear.2004.09.041>
26. S.A. Alidokht, P. Manimunda, P. Vo, S. Yue, and R.R. Chromik, Cold Spray Deposition of a Ni-WC Composite Coating and Its Dry Sliding Wear Behavior, *Surf. Coat. Technol.*, 2016, **308**, p 424–434. <https://doi.org/10.1016/j.surfcoat.2016.09.089>
27. J. Ziegelheim, L. Lombardi, Z. Cesanek, S. Houdkova, J. Schubert, D. Jech, L. Celko, and Z. Pala, Abradable Coatings for Small Turboprop Engines: A Case Study of Nickel-Graphite Coating, *J. Therm. Spray Technol.*, 2019, **28**, p 794–802. <https://doi.org/10.1007/s11666-019-00838-4>
28. C.G. Xu, L.Z. Du, B. Yang, and W.G. Zhang, Study on Salt Spray Corrosion of Ni-Graphite Abradable Coating with 80Ni20Al and 96NiCr-4Al as Bonding Layers, *Surf. Coat. Technol.*, 2011, **205**, p 4154–4161. <https://doi.org/10.1016/j.surfcoat.2011.03.007>

**Publisher's Note** Springer Nature remains neutral with regard to jurisdictional claims in published maps and institutional affiliations.